Systems & Control Transactions

Research Article - Peer Reviewed Conference Proceeding
ESCAPE 35 - European Symposium on Computer Aided Process Engineering
Ghent, Belgium. 6-9 July 2025
Jan F.M. Van Impe, Grégoire Léonard, Satyajeet S. Bhonsale,
Monika E. Polańska, Filip Logist (Eds.)

PSE PRESS

Modelling of the Co-precipitation of Ni-Mn-Co Hydroxides.

Erik G. Resendiz-Mora[a], and Solomon F. Brown[a]*

[a] University of Sheffield, Department of Chemical and Biological Engineering, Sheffield, South Yorkshire, United Kingdom
* Corresponding Author: s.f.brown@sheffield.ac.uk.

ABSTRACT

A simple mathematical model of the co-precipitation of Ni-Mn-Co hydroxides is developed and applied to investigate the effect of pH, initial concentration of ammonia in the solution, concentration of the ammonia feed, nucleation rate constant and exponent, growth rate constant and growth exponent over the model output. The model is shown to produce a correct representation of the precipitation variables, and the general trends obtained for different sets of parameters are found in agreement with results presented elsewhere. A sensitivity analysis is carried out and the sensitivity indices are calculated. It is found that pH, initial concentration of ammonia and growth rate constant are the input parameters with the most relevant effect over the model input.

Keywords: Aspen Custom Modeler, Co-precipitation modeling, Ni-Mn-Co hydroxide, Cathode precursor.

INTRODUCTION

As the world transitions to cleaner energy sources like solar and wind, which are inherently intermittent, lithium-ion batteries have emerged as a suitable solution due to their high energy density, versatility, and long cycle life. Li-ion batteries excel in storing excess energy generated during periods of high production and releasing it when supply falls short, enabling a stable and reliable energy supply. Widely used in portable electronics, electric vehicles, and stationary energy storage systems [1-4], lithium-ion batteries also play a pivotal role in the electrification of transportation, significantly reducing reliance on fossil fuels and lowering greenhouse gas emissions. Their integration into energy systems not only facilitates the adoption of renewable energy but also supports global efforts to achieve net-zero carbon goals. By bridging the gap between energy production and consumption, lithium-ion batteries are indispensable in building a sustainable and resilient energy future.

The widespread adoption of batteries in daily life faces significant challenges, particularly regarding performance, cost, and sustainability. A key hurdle lies in optimizing cathode materials, which critically influence a battery's energy density, lifespan, and overall efficiency [5, 6]. These properties are largely inherited from the chosen materials for cathode's precursors and from the synthesis route, which determines relevant features of the particles such as their mean size, PSD, porosity and morphology.

Ni-Mn-Co hydroxides can be synthesized by different methods, e.g. solvo/hydrothermal, solid state, or co-precipitation [5, 7, 8]. The latter involves the mixing of stoichiometric amounts of transition metal salts with a complexing agent (e.g. ammonia) and a precipitating agent (e.g. sodium hydroxide) under controlled reaction conditions to produce quasi-spherical particles and tailor the particle morphology and density. Key parameters to optimize such particle properties are the reaction environment pH, stirring velocity, temperature and reaction time [5, 9, 10].

The optimization of the parameters mentioned above can be troublesome, particularly because the precipitation environment is very scale-dependent and an observed behaviour at a lab facility might not be reproduced at an industrial precipitator, hence, following an experimental route may prove costly and ineffective [11]. To tackle this problem, it is useful to turn to mathematical models that can produce a fair representation of the phenomena at a low cost. Because of that, in this investigation we develop a mathematical model of a semi-batch precipitator to study the effect of input parameters in the response of the model regarding the particle size distribution (PSD), the supersaturation and the particle mean

sizes $d_{4,3}$ and $d_{3,2}$. A few studies regarding the modelling of co-precipitation of Ni-Mn-Co hydroxides are available in the open literature. Barai et al. [2] developed a multi-scale model considering nucleation, growth and aggregation of particles and simulated a continuous stirred tank crystallizer to study the effect of pH and ammonia concentration over the PSD and mean particle size. Shiea et al. [1] applied a CFD-PBE modelling approach to a multi-inlet vortex micromixer and simulated the effect of varying the flowrate and concentration of the feed, they reported a decrease in mean particle size as the feed concentration and flowrate increase. Para et al. [3] applied the same approach to simulate a similar system and fitted the model output to experimental datapoints of mean particle size. Mugumya et al. [12] investigated the co-precipitation of NMC111; their modelling work was limited to solving the equilibrium conditions and did not include any description of the formation and growth of crystals. Querio et al. [13] compared the computational performance of the CFD-PM approach versus a compartment model and found that the latter approach render less accurate, yet less computationally expensive qualitatively correct predictions. In this work, we utilize a simple transient model of a semi-batch crystallizer to study the sensitivity of the response of the model to the variation of relevant operating parameters like pH and ammonia concentration, but also to the changes of the kinetic parameters of crystal nucleation and growth. The intent of this work is to obtain a simple, representative model capable of producing a reliable output regarding PSD and particle size, which will be integrated in the context of a whole manufacturing plant model in future work.

METHODS

System description

The system to be modelled is a stirred crystallizer operating in a semi-batch mode as illustrated in Figure 1. The crystallizer is initially charged with a solution of aqueous ammonia prepared according to the specifications outlined in Table 1. During the process, a 2M transition metal solution containing an 8:1:1 ratio of nickel, manganese and cobalt is gradually introduced into the reactor, along with a 10M sodium hydroxide solution and an aqueous ammonia solution with concentration varying from 1.14 – 5.7M. The operating parameters of the crystallizer are summarized in Table 1.

Model assumptions.

The development of the crystallizer model is based on the following key assumptions, which simplify the representation of the system while maintaining its relevance to practical applications:

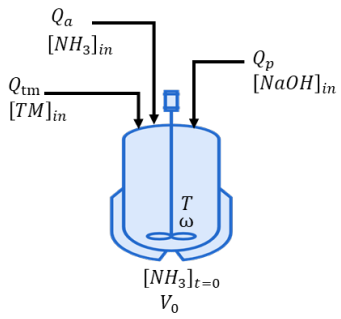

Figure 1. Schematic representation of the modelled crystallyzer.

Table 1: Operating conditions of the crystallizer.

Param.	Description	Value
T	Temperature	60°C
ω	Stirring velocity	1000 rpm
V_0	Initial solution volume	0.0008 m^3
$[TM]$	Molar concentration of the transition metal solution.	2M
$[NaOH]$	Molar concentration of the precipitating agent.	10M
Q_{TM}	TM solution volumetric flowrate	$4.8x10^{-5}$ m^3 h^{-1}
Q_a	Chelating agent sol. volumetric flowrate	$2.4x10^{-5}$ m^3 h^{-1}
Q_p	Precipitating agent sol. volumetric flowrate.	$1.92x10^{-5}$ m^3 h^{-1}
t_a	Reagent addition time.	10.4h

1. Crystal particles are modeled as having spherical geometries to streamline the mathematical treatment of shape-dependent phenomena.
2. The formation of transition metal hydroxides is considered negligible. The primary reaction pathway is assumed to involve the formation of transition metal ion complexes, followed by their conversion into combined transition metal hydroxides.
3. The reaction rates for both ionic complex formation and hydroxide formation are assumed to be fast. As a result, the rate-controlling processes are the nucleation and growth of crystals.
4. Aggregation and breakage of crystals are neglected, focusing the model on the nucleation and growth mechanisms.
5. The crystallizer is assumed to operate isothermally, with a consistent and uniform temperature maintained throughout the process.
6. It is assumed that no seed crystals are present in the feed entering the crystallizer.

Model development.

The particle size distribution is mathematically described by the population balance equation (PBE). For a semi-batch crystallizer, the PBE is [14]:

$$\frac{\partial Vn}{\partial t} + G\frac{\partial Vn}{\partial L} = 0 \quad (1)$$

Where V is the crystallizer volume, n is the number density, t is the batch time, L is the crystal size and G is the crystal growth rate. Equation (1) neglects the agglomeration and breakage of particles in the crystallizer. Since the crystallization process starts from a clear solution, the following initial condition applies to Equation (1):

$$n(0, L) = 0 \quad (2)$$

Additionally, the following boundary condition is applied depending on the level of supersaturation of the desired product in the crystallizer:

$$n(t, 0) = \begin{cases} 0 \; if \; S \leq 1 \\ \frac{B}{G} \; if \; S > 1 \end{cases} \quad (3)$$

Where S is the supersaturation and B is the nucleation rate; the supersaturation, and by extension the nucleation and growth rates relate to the equilibrium concentration of the ions of nickel ($[Ni^{2+}]_{eq}$), manganese ($[Mn^{2+}]_{eq}$), cobalt ($[Co^{2+}]_{eq}$), and hydroxyl ions ($[OH^-]$) and are defined as:

$$S = \left(\frac{[Ni^{2+}]_{eq}^{x}[Mn^{2+}]_{eq}^{y}[Co^{2+}]_{eq}^{z}[OH^-]_{eq}^{2}}{K_{sp}^{Ni_xMn_yCo_z(OH)_2}} \right)^{1/3} \quad (4)$$

$$B = k_B(S-1)^b \quad (5)$$

$$G = k_G(S-1)^g \quad (6)$$

Where k_B is the nucleation kinetic constant, k_G is the growth kinetic constant, b is the nucleation exponent, g is the growth exponent and the exponents x, y and z are determined by the desired stoichiometry of the combined hydroxide; for the case of NMC811, these values are $x = 0.8$, $y = 0.1$ and $z = 0.1$. The equilibrium concentrations of the ionic species in the solution are calculated by solving the complex chemical equilibrium relationships expressed in Equations (7) – (13):

$$[Ni^{2+}] = [Ni^{2+}]_{eq} + \sum_{i=1}^{6}\left[Ni(NH_3)_n{}^{2+}\right]_{eq} \quad (7)$$

$$[Mn^{2+}] = [Mn^{2+}]_{eq} + \sum_{i=1}^{4}\left[Mn(NH_3)_n{}^{2+}\right]_{eq} \quad (8)$$

$$[Co^{2+}] = [Co^{2+}]_{eq} + \sum_{i=1}^{6}\left[Co(NH_3)_n{}^{2+}\right]_{eq} \quad (9)$$

$$[NH_3] = [NH_3]_{eq} + [NH_4^+]_{eq} + \sum_{n=1}^{6} n\left[Ni(NH_3)_n{}^{2+}\right]_{eq} + \sum_{n=1}^{4} n\left[Mn(NH_3)_n{}^{2+}\right]_{eq} + \sum_{n=1}^{6} n\left[Co(NH_3)_n{}^{2+}\right]_{eq} \quad (10)$$

$$K_n^{M^{2+}} = \frac{\left[M(NH_3)_n{}^{2+}\right]_{eq}}{[M^{2+}]_{eq}[NH_3]_{eq}^{n}} \quad (11)$$

$$K_w = [H_3O^+]_{eq}[OH^-]_{eq} \quad (12)$$

$$K_b = \frac{[NH_4^+]_{eq}[OH^-]_{eq}}{[NH_3]_{eq}} \quad (13)$$

Where the equilibrium constants of the coordination of transition metal ions with ammonia ($K_n^{M^{2+}}$), the dissociation of water (K_w), and dissociation of ammonia (K_b) are taken from [15]. To solve Equations (7) – (13) the total concentrations of nickel ($[Ni^{2+}]$), manganese ($[Mn^{2+}]$), cobalt ($[Co^{2+}]$), and ammonia ($[NH_3]$) are required; the concentration of these species evolve dynamically throughout the process and are given by:

$$\frac{d[Ni^{2+}]V}{dt} = Q_{tm}[Ni^{2+}]_{in} - \frac{0.8Vk_v\rho_c}{MW_c}\frac{dm_3}{dt} \quad (14)$$

$$\frac{d[Mn^{2+}]V}{dt} = Q_{tm}[Mn^{2+}]_{in} - \frac{0.1Vk_v\rho_c}{MW_c}\frac{dm_3}{dt} \quad (15)$$

$$\frac{d[Co^{2+}]V}{dt} = Q_{tm}[Co^{2+}]_{in} - \frac{0.1Vk_v\rho_c}{MW_c}\frac{dm_3}{dt} \quad (16)$$

$$\frac{d[SO_4^{2-}]V}{dt} = Q_{tm}[SO_4^{2-}]_{in} \quad (17)$$

$$\frac{d[NH_3]V}{dt} = Q_a[NH_3]_{in} \quad (18)$$

$$\frac{d[Na^+]V}{dt} = Q_p[Na^+]_{in} \quad (19)$$

$$\frac{dV}{dt} = Q_s + Q_a + Q_p \quad (20)$$

$$\frac{dm_3}{dt} = 3Gm_2 \quad (21)$$

$$m_2 = \int_0^{\infty} n\,L^2 dL \quad (22)$$

Where Q_s, Q_a, and Q_p are the volumetric flowrates of transition metal solution, ammonia and precipitant agent; k_v is the volumetric factor, ρ_c is the crystal density, MW_c is the precipitate molecular weight, m_2 and m_3 are the second and third moments of the particle size distribution.

Model solution.

The model equations were implemented and solved using the method of lines in Aspen Custom Modeler. A total of 250 simulations were conducted, varying key parameters, including the initial concentration of ammonia, the ammonia concentration fed to the crystallizer, the solution pH, and the crystallization kinetics parameters for crystal nucleation and growth. These variables were randomly sampled using the Latin hypercube sampling method, ensuring efficient exploration of the parameter space within the ranges specified in Table 2.

RESULTS

The results of the simulation of four selected cases for key variables like supersaturation, mean particle sizes and particle size distribution are presented in Figures 2 through 5. As mentioned before, the input parameters

utilized for these simulations were randomly sampled, and for quick reference are presented in Table 3.

Table 2: Parameter ranges utilized to simulate the co-precipitation of Ni-Mn-Co hydroxides.

Param.	Description	Value
$[NH_3]_{t=0}$	Initial ammonia conc.	0.3–1.5M
$[NH_3]_{in}$	Ammonia feed conc.	1.14–5.7M
pH	Solution pH	9.5–11.5
k_B	Nucleation constant	10^4–10^{10}
b	Nucleation exponent	1–5
k_G	Growth constant	10^{-6}–10^{-10}
g	Growth exponent	0.5 – 2.5

Table 3: Input parameters utilized to generate the results presented in this paper.

Param	Units	(a)	(b)	(c)	(d)
$[NH_3]_{t=0}$	mol m^{-3}	1.17	0.51	0.74	0.63
$[NH_3]_{in}$	mol m^{-3}	3.32	1.66	2.43	3.79
pH	-	11.4	9.9	9.8	10.2
$k_B x10^{-6}$	$m^{-3}\,h^{-1}$	0.014	22.3	0.057	0.131
b	-	4.5	2.8	4.7	4.0
$k_G x10^{10}$	$m\,h^{-1}$	81.7	27.0	3.7	3.44
g	-	1.0	1.5	2.4	1.7

Figure 2 presents multiple supersaturation profiles generated by the model using different sets of input parameters. As anticipated for a semi-batch system initially containing only one of the reacting species, the supersaturation levels increase over time, reaching a peak before gradually declining until the end of the process.

In all cases, an initial induction period is observed at the start of the run, marking the addition of reagents to the crystallizer. After this phase, supersaturation breaks through and builds up at a rate dictated by crystallization kinetics and reactant concentrations. The magnitude of supersaturation is determined by the availability of transition metal and hydroxyl ions in the solution [1], with the highest levels in Figure 2 corresponding to simulation cases with the highest pH. Conversely, the position of the supersaturation peak is influenced by crystallization kinetics, particularly the crystal growth rate, which governs how quickly reactants are consumed to form Ni-Mn-Co hydroxide crystals.

Figures 3 and 4 are plots of the evolution of the volume-weighted mean size and the surface-weighted mean size, respectively. In both cases, the growth of the NMC particles breaks trough after 3 hours which coincides with the development of the supersaturation curves discussed above. For Case (a), both the volume- and surface-weighted mean sizes seem to have an initially fast growth but then plateau at the lowest mean size of the four cases. Conversely, for case (c) the growth is sustained for longer, yielding the highest mean particle sizes among all of them. This behaviour seems obvious given the rapid decline of the supersaturation for case (a), which in turn renders a decline of the crystal growth rate. On the other hand, for case (c), even when the supersaturation does not reach very high values, its decline is less severe and, in addition, the value of the growth exponent magnifies the crystal growth rate.

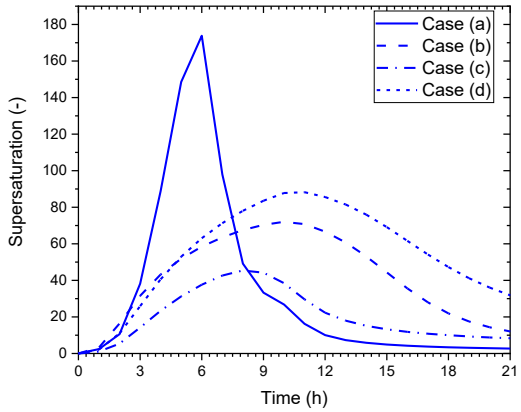

Figure 2. Supersaturation of Ni-Mn-Co hydroxide at different operating conditions of pH and ammonia concentration, and with different sets of kinetic parameters.

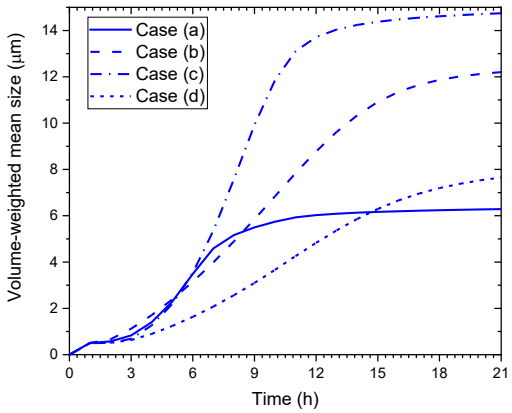

Figure 3. Volume-weighted mean size of the selected numerical experiments simulated.

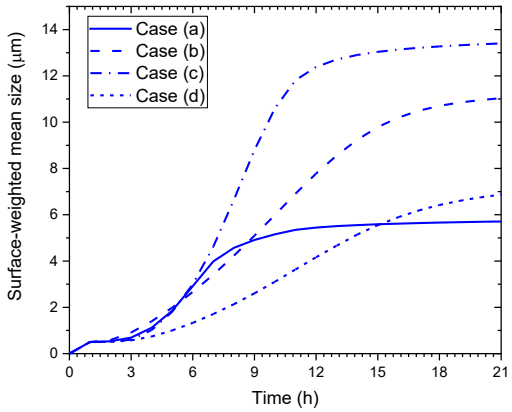

Figure 4. Surface-weighted mean size of the selected numerical experiments simulated.

Figure 5 displays the particle size distribution (PSD) for simulation cases (a), (b), (c), and (d), highlighting the significant impact of varying input parameters. All PSD curves exhibit unimodal distributions skewed toward the smaller particle size range, with a decreasing coefficient of variation as pH increases. The coefficient of variation refers to the 'width' of the distribution and it reflects the degree of polydispersity in crystal size; in the results presented here, the most uniform product is achieved at pH 11.5, albeit with the smallest particle size. The trends identified align with previous studies [2], albeit the optimal pH condition depend upon the desired product to be synthesized [5].

Determining the importance of the input parameters is complex due to the interplay among factors both physically and in the mathematical model. To support the investigation of the relevance of the input parameters, the sensitivity indices were calculated and are presented in Table 4. This analysis was carried out considering the mean sizes $d_{4,3}$ and $d_{3,2}$ as the outputs of interest. By inspecting the values summarized in Table 4, it is evident that the k_G, g, pH and $[NH_3]_{t=0}$ have a strong influence over the output of the model.

Table 4: Sensitivity indices of the investigated parameters.

Parameter	Indices
$[NH_3]_{t=0}$	0.1341
$[NH_3]_{in}$	0.0036
pH	0.0809
k_B	0.0001
b	0.0023
k_G	0.6378
g	0.1413

CONCLUSIONS

A simple mathematical model of a semi-batch crystallizer has been presented. The model has been solved by the method of lines utilizing the commercial solver contained in Aspen Custom Modeler® and applied to conduct a sensitivity and uncertainty analysis to verify the effect of pH and ammonia concentration, and the kinetics of nucleation and growth over the particle size distribution and mean particle sizes.

Despite the simplicity of the model, it produces a fair representation of the precipitation variables, and the prediction of relevant particle properties agrees with the observations of previous work conducted for this type of system. The model can be enhanced by incorporating the

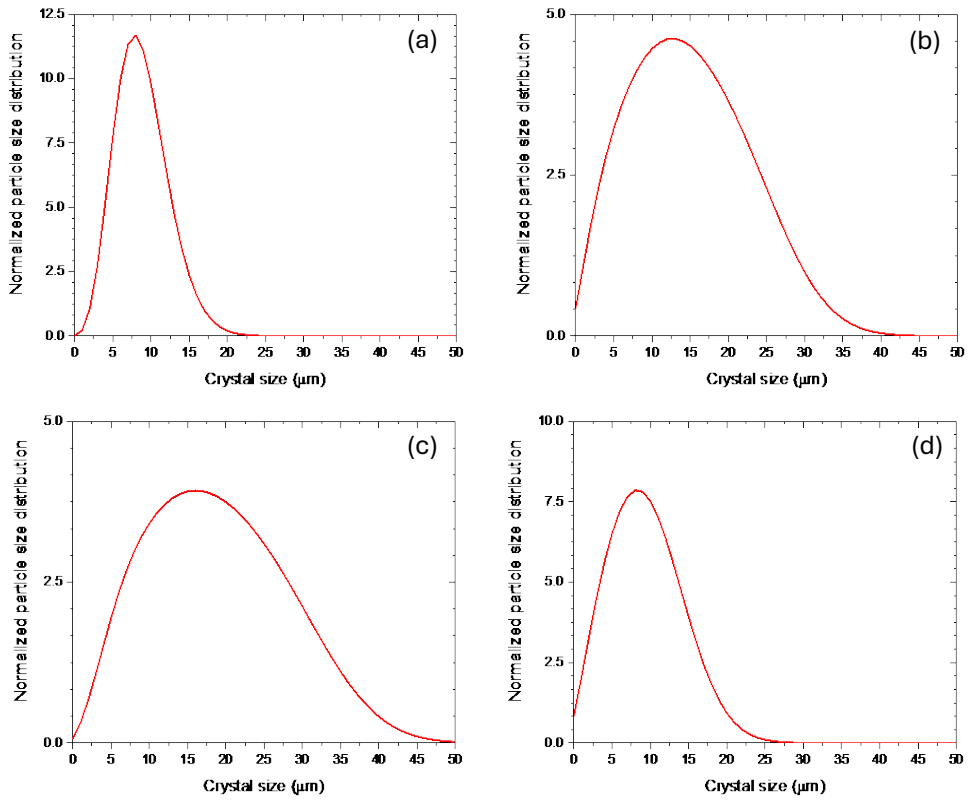

Figure 5: Particle size distribution (PSD) curves of selected numerical experiments simulated in this work.

aggregation/breakage phenomena into the PBE and by incorporating the thermal effects over the crystallization kinetics.

The sensitivity analysis indices indicated that the crystallization of Ni-Mn-Co hydroxides with stoichiometry 0.8:0.1:0.1 is primarily sensitive to the growth kinetics, the solution pH and the initial concentration of ammonia. Less relevant is the kinetics of nucleation, whereas the concentration of ammonia feed seems to be irrelevant.

FUTURE WORK

The resulting model is to be improved by incorporating the agglomeration/breakage term to the population balance. Similarly, the effect of temperature over the crystallization kinetics was not incorporated in this work, this is an important piece to enable a better understanding and optimization of the process. This model will be used to conduct studies regarding the kinetics of crystallization.

ACKNOWLEDGEMENTS

The authors would like to thank the UK Engineering and Physical Sciences Research Council (EPSRC) for funding the SuMMa project, grant reference EP/W018950/1.

REFERENCES

1. Shiea, M., et al., CFD-PBE modelling of continuous Ni-Mn-Co hydroxide co-precipitation for Li-ion batteries. Chemical Engineering Research & Design, 2022. 177: p. 461-472.
2. Barai, P., et al., Multiscale Computational Model for Particle Size Evolution during Coprecipitation of Li-Ion Battery Cathode Precursors. Journal of Physical Chemistry B, 2019. 123(15): p. 3291-3303.
3. Para, M.L., et al., A modelling and experimental study on the co-precipitation of Ni_{0.8}Mn_{0.1}Co_{0.1}(OH)₂ as precursor for battery cathodes. Chemical Engineering Science, 2022. 254.
4. Wu, Z.W., et al., Investigating the effect of pH on the growth of coprecipitated Ni0.8Co0.1Mn0.1(OH)2 agglomerates as precursors of cathode materials for Li-ion batteries. Ceramics International, 2023. 49(10): p. 15851-15864.
5. Entwistle, T., et al., Co-precipitation synthesis of nickel-rich cathodes for Li-ion batteries. Energy Reports, 2022. 8: p. 67-73.
6. Enasel, E. and G. Dumitrascu, Storage solutions for renewable energy: A review. Energy Nexus, 2025. 17.
7. Breddemann, U. and I. Krossing, Review on Synthesis, Characterization, and Electrochemical Properties of Fluorinated Nickel-Cobalt-Manganese Cathode Active Materials for Lithium-Ion Batteries. Chemelectrochem, 2020. 7(6): p. 1389-1430.
8. Pardikar, K., et al., Status and outlook for lithium-ion battery cathode material synthesis and the application of mechanistic modeling. Journal of Physics-Energy, 2023. 5(2).
9. Han, Q.Y., et al., Study on the Effect of Coprecipitation Conditions on the Growth and Agglomeration of Ni_{0.8}Co_{0.1}Mn_{0.1}(OH)₂ Particles. Industrial & Engineering Chemistry Research, 2024. 64(1): p. 283-300.
10. Lee, M.H., et al., Synthetic optimization of Li Ni_{1/3}Co_{1/3}Mn_{1/3} O₂ via co-precipitation. Electrochimica Acta, 2004. 50(4): p. 939-948.
11. Mou, M.Y., et al., Scalable Advanced Li(Ni0.8Co0.1Mn0.1)O2 Cathode Materials from a Slug Flow Continuous Process. Acs Omega, 2022. 7(46): p. 42408-42417.
12. Mugumya, J.H., et al., Synthesis and Theoretical Modeling of Suitable Co-precipitation Conditions for Producing NMC111 Cathode Material for Lithium-Ion Batteries. Energy & Fuels, 2022. 36(19): p. 12261-12270.
13. Querio, A., et al., Comparison between Compartment and Computational Fluid Dynamics Models for Simulating Reactive Crystallization Processes. Industrial & Engineering Chemistry Research, 2024. 63(50): p. 21991-22004.
14. Jha, S.K., S. Karthika, and T.K. Radhakrishnan, Modelling and control of crystallization process. Resource-Efficient Technologies, 2017. 3(1): p. 94-100.
15. van Bommel, A. and J.R. Dahn, Analysis of the Growth Mechanism of Coprecipitated Spherical and Dense Nickel, Manganese, and Cobalt-Containing Hydroxides in the Presence of Aqueous Ammonia. Chemistry of Materials, 2009. 21(8): p. 1500-1503.